FINITE ELEMENT/LEVEL SET MODELING OF SURFACE TENSION WITH MARANGONI EFFECTS AND DYNAMIC CONTACT LINES

Gustavo C. Buscaglia and Roberto F. Ausas

Instituto de Ciências Matemáticas e Computação, Universidade de São Paulo, Av. do Trabalhador Sãocarlense 400, 13560-970 São Carlos, SP, Brazil, rfausas@gmail.com

Keywords: Surface tension, Marangoni forces, Laplace–Beltrami, Finite elements, Contact lines, Variational formulations.

Abstract. In this work we provide a complete variational framework for the modeling of capillary effects, starting from the virtual-work principle and arriving at a variational formulation suitable for numerical treatment by means of the finite element method. This formulation is then coupled with a level-set representation of the interface and suitable approximation spaces and stabilization terms. An interesting aspect is that the Marangoni force arising from surface tension gradients is automatically incorporated. This is illustrated by solving the thermocapillary migration of a droplet under a constant temperature gradient, which has an analytical solution. The treatment of contact lines is also addressed from within the variational framework, in particular the imposition of the static contact angle and of local dissipation laws. Some numerical examples of spreading drops are used to clarify controversial issues of this challenging problem.

1   INTRODUCTION

The physics of surface tension, capillarity and wetting/dewetting phenomena is a very vast and active field of research for which a classical reference is the work of de Gennes et al. (2004), while an update of the state of the art can be found in the article of Bonn et al. (2009).

Over the years, a large volume of information has been published about the *numerical simulation of flows with interfaces*, of which review articles can be found (Scardovelli and Zaleski, 1999; Sethian and Smereka, 2003; Tezduyar, 2007; Fuster et al., 2009; Idelsohn et al., 2009; Mc Kee et al., 2008). These works consider either a passive interface or a capillary one, in which surface tension forces have been accounted for. However, capillary forces are introduced axiomatically, with little or no discussion of their physical and mechanical interpretation.

On the other hand, there is a growing interest in microscopic flows with quite complex interfaces. Textured, superhydrophobic and electrically modifiable surfaces have already entered microfluidic technologies (Rothstein, 2010; Squires and Quake, 2005; Stone et al., 2004), and the study and manipulation of complex colloids and biological interfaces is now within reach (Kim et al., 2009; Whitesides, 2006; Squires and Mason, 2010). Successful numerical modeling of interfaces of such complexity cannot be performed without mechanical intuition and understanding. In fact, current research in elastic and geometric biomembranes is fundamentally based on energy considerations (Skalak et al., 1973; Marella and Udaykumar, 2004; Lac et al., 2004; Pozrikidis, 2003; Breyiannis and Pozrikidis, 2000; Bonito et al., 2010; Dziuk, 2008).

The plan for this article is to analyze the energetics of capillary phenomena from the viewpoint of the virtual–work principle, so as to translate the well-established physics (see, e.g., de Gennes et al. (2004)) into a language more familiar to practicioners of Computational Mechanics. For this purpose, we first focus on a variational derivation of the virtual work $\mathcal{P}_\Gamma$ associated with the deformation of the interface Γ, which is the only difference with respect to the classical Stokes problem when Γ is closed, and then extend the analysis to problems with contact lines, in which as we will see both $\mathcal{P}_\Gamma$ and $\mathcal{P}_{\partial\Omega}$ play crucial roles. The derivation purposely contains all required mathematical proofs in a seldom used but very practical framework that does not require covariant differentiation (Secomb and Skalak, 1982). Along the analysis, connections to previous mathematical and numerical formulations are made, so as to discuss current practices from the proposed viewpoint, and some challenging open problems are identified.

2   MATHEMATICAL FORMULATION

In this article, we focus on surface–tension phenomena involving two incompressible Newtonian fluids at scales small enough for inertial and gravitational effects to be negligible. We consider the flow of these fluids in a domain Ω which for simplicity is assumed bounded by a rigid, impenetrable solid (its boundary is denoted by $\partial\Omega$, also assumed smooth). The domain Ω splits into two subdomains, Ω_+ occupied by fluid A and Ω_- occupied by fluid B. The interface between Ω_+ and Ω_- is denoted by Γ, which is assumed to be a smooth surface that can either be closed or have a boundary $\partial\Gamma$ at which there exists fluid/fluid/solid contact (the well-known "contact line"). It is also assumed that there is no slip between the fluids at the interface, so that a global velocity field $\mathbf{u} \in (H^1(\Omega))^d$ can be defined. A global pressure $p \in L^2(\Omega)$ is also defined, and the viscosity $\mu(\mathbf{x})$ is taken as $\mu_A(\mathbf{x})$ if $\mathbf{x} \in \Omega_+$ and as $\mu_B(\mathbf{x})$ if $\mathbf{x} \in \Omega_-$.

Introducing the spaces

$$W \;\dot{=}\; \{\mathbf{w} \in (H^1(\Omega))^d \mid \mathbf{w} \cdot \check{\mathbf{n}} = 0 \;\text{ at } \partial\Omega\} \tag{1}$$

$$Q \;\dot{=}\; L^2(\Omega)/\mathbb{R} \tag{2}$$

the variational formulation of the problem reads: *Find* $(\mathbf{u}, p) \in W \times Q$ *such that*

$$\int_\Omega 2\mu \, D\mathbf{u} : D\mathbf{w} \, d\Omega - \int_\Omega p \, \nabla \cdot \mathbf{w} \, d\Omega \;=\; \int_\Omega \mathbf{b} \cdot \mathbf{w} \, d\Omega + \mathcal{P}_{\partial\Omega}(\mathbf{w}) + \mathcal{P}_\Gamma(\mathbf{w}) \tag{3}$$

$$\int_\Omega q \, \nabla \cdot \mathbf{u} \, d\Omega \;=\; 0 \tag{4}$$

for all $(\mathbf{w}, q) \in W \times Q$. In (3) $\mathbf{b}$ is a volume force.

Because W admits tangential movement of the fluid with respect to $\partial\Omega$, a linear form $\mathcal{P}_{\partial\Omega} : W \to \mathbb{R}$ has been introduced expressing the virtual work at the boundary. Similarly, $\mathcal{P}_\Gamma$ is a linear form expressing the virtual work associated to the interface Γ. The physical and mathematical meaning of these forms, which may depend on $\mathbf{u}$ or other variables, will be thoroughly discussed in the next sections, for the time being it suffices to accept that (3)–(4) is a well-posed variational problem whenever the right-hand side of (3) is linear and continuous in W. Notice that the time enters the mathematical problem parametrically.

2.1 Virtual work of surface tension

Consider a surface Γ at which there exists a heterogeneity in the composition or structure, leading to a corresponding energy $\mathcal{E}(\Gamma)$. Assuming this energy to be additive, it can be written as

$$\mathcal{E}(\Gamma) = \int_\Gamma \gamma(\mathbf{x}) \, d\Gamma \tag{5}$$

where γ is a surface energy density that could depend on many variables, such as the deformation with respect to some relaxed configuration (as in elastic interfaces) or the local curvature of the interface (as in lipidic membranes), as long as γ satisfies some basic locality and objectivity principles.

The simplest constitutive behavior for γ is, of course, that the surface energy density is a constant, depending just on the material identity of the point $\mathbf{x}$. To further simplify the model, it can also be assumed that there is no localized dissipation at Γ. The virtual work corresponding to a velocity field $\mathbf{w}$ is thus equal to minus the rate of change of $\mathcal{E}(\Gamma)$ when Γ is virtually displaced following $\mathbf{w}$ (in other words, $-\mathcal{P}_\Gamma$ equals the shape derivative of $\mathcal{E}(\Gamma)$ along the vector field $\mathbf{w}$).

Let $\mathbf{v}$ be a vector field defined on Γ. It defines the one–parameter family of transformations

$$\boldsymbol{\varphi}_\mathbf{v} : \Gamma \times] - s_0, s_0[\to \Omega, \qquad \boldsymbol{\varphi}_\mathbf{v}(\mathbf{x}, s) = \mathbf{x} + s \, \mathbf{v}(\mathbf{x}) \tag{6}$$

which transform Γ into the family of perturbed surfaces

$$\Gamma_{\mathbf{v},s} \doteq \{\mathbf{y} \in \Omega \mid \mathbf{y} = \mathbf{x} + s \, \mathbf{v}(\mathbf{x}), \; \mathbf{x} \in \Gamma\} \tag{7}$$

The energy of the perturbed surface $\Gamma_{\mathbf{v},s}$ is,

$$\mathcal{E}(\Gamma; \mathbf{v}, s) = \int_\Gamma \gamma(\mathbf{x}) \, J_\Gamma(\mathbf{x}, s) \, d\Gamma \tag{8}$$

where $J_\Gamma(\mathbf{x}, s) = d\Gamma_{\mathbf{v},s}/d\Gamma$ is the surface Jacobian at $\mathbf{x}$ of the transformation $\boldsymbol{\varphi}_\mathbf{v}(\cdot, s)$.

Now, we define the shape derivative of $\mathcal{E}(\Gamma)$ in a precise manner as

$$d\mathcal{E}(\Gamma; \mathbf{v}) \doteq \lim_{s \to 0} \frac{\mathcal{E}(\Gamma; \mathbf{v}, s) - \mathcal{E}(\Gamma)}{s} \tag{9}$$

To compute (9) we need to introduce several tools.

First, the transformation $\boldsymbol{\varphi}_{\mathbf{v}}$ can be extended out of Γ as

$$\widehat{\boldsymbol{\varphi}}_{\mathbf{v}}(\mathbf{x}, s) = \mathbf{x} + s\,\widehat{\mathbf{v}}(\mathbf{x}) \tag{10}$$

where $\widehat{\mathbf{v}}(\mathbf{x})$ is the normal extension of $\mathbf{v}$, i.e.

$$\widehat{\mathbf{v}}(\mathbf{x}) \;\doteq\; \mathbf{v}(\Pi_\Gamma(\mathbf{x})) \tag{11}$$

Equation (10) is a 3D deformation to which the well–known formulae from Continuum Mechanics (Gurtin, 1981) apply. We also decompose $\widehat{\mathbf{v}}(\mathbf{x})$ into its normal and tangential components as

$$\widehat{\mathbf{v}} = \widehat{v}_n\,\widehat{\mathbf{n}} + \widehat{\mathbf{v}}_\tau \tag{12}$$

Keeping $\mathbf{v}$ and s fixed and omitting them from the notation, we have, in particular (notice that the developments are truncated to first order in s)

$$\mathbf{F} \;\doteq\; \nabla\widehat{\boldsymbol{\varphi}} = \mathbb{I} + s\nabla\widehat{\mathbf{v}} = \mathbb{I} + s(\widehat{\mathbf{n}} \otimes \nabla\widehat{v}_n + \widehat{v}_n\,\nabla\widehat{\mathbf{n}} + \nabla\widehat{\mathbf{v}}_\tau) \tag{13}$$

$$\mathbf{F}^{-1} \;=\; \mathbb{I} - s\,\nabla\widehat{\mathbf{v}} = \mathbb{I} - s(\widehat{\mathbf{n}} \otimes \nabla\widehat{v}_n + \widehat{v}_n\,\nabla\widehat{\mathbf{n}} + \nabla\widehat{\mathbf{v}}_\tau) \tag{14}$$

$$J \;\doteq\; \det\mathbf{F} = 1 + s\,\nabla\cdot\widehat{\mathbf{v}} = 1 + s(\widehat{v}_n\nabla\cdot\widehat{\mathbf{n}} + \nabla\cdot\widehat{\mathbf{v}}_\tau) \tag{15}$$

Now, letting $\mathbf{dA} = \check{\mathbf{n}}\,d\Gamma$ denote the area differential vector and $\mathbf{da}$ its image by $\boldsymbol{\varphi}$, it is known that

$$\mathbf{da} = J\,(\mathbf{F}^{-1})^T\,\mathbf{dA} \tag{16}$$

and thus

$$\mathbf{da} \;=\; (1 + s\,\nabla\cdot\widehat{\mathbf{v}})\,\mathbf{dA} - s\,\nabla\widehat{\mathbf{v}}^T\,\mathbf{dA} \tag{17}$$

$$=\; [1 + s(\widehat{v}_n\,\nabla\cdot\widehat{\mathbf{n}} + \nabla\cdot\widehat{\mathbf{v}}_\tau)]\,\mathbf{dA} - s[\nabla\widehat{v}_n \otimes \widehat{\mathbf{n}} + (\nabla\widehat{\mathbf{v}}_\tau)^T]\,\mathbf{dA} \tag{18}$$

where we have used $\nabla\widehat{\mathbf{n}}\cdot\widehat{\mathbf{n}} = 0$. It can be verified that the first term on the right-hand side of (17) (or equivalently (18)) is normal to Γ, while the second term is tangential. Thus, to first order in s, since $d\Gamma_{\mathbf{v},s} = \|\mathbf{da}\|$ we have

$$d\Gamma_{\mathbf{v},s} = (1 + s\,\nabla\cdot\widehat{\mathbf{v}})\,d\Gamma = [1 + s(\widehat{v}_n\,\nabla\cdot\widehat{\mathbf{n}} + \nabla\cdot\widehat{\mathbf{v}}_\tau)]\,d\Gamma \tag{19}$$

which combined with (8) and (9) leads to

$$d\mathcal{E}(\Gamma;\mathbf{v}) = \int_\Gamma \gamma\,\nabla\cdot\widehat{\mathbf{v}}\,d\Gamma = \int_\Gamma \gamma\,(\widehat{v}_n\,\nabla\cdot\widehat{\mathbf{n}} + \nabla\cdot\widehat{\mathbf{v}}_\tau)\,d\Gamma \tag{20}$$

Integration-by-parts formulae

The following integration-by-parts formulae hold (see Buscaglia and Ausas (2011)). For any f defined and differentiable on Γ,

$$\int_\Gamma \nabla_\Gamma f\,d\Gamma = \int_\Gamma f\,\kappa\,\check{\mathbf{n}}\,d\Gamma + \int_{\partial\Gamma} f\,\check{\boldsymbol{\nu}}\,d\partial\Gamma \tag{21}$$

so that, applying it componentwise, we get for any tangentially differentiable vector field $\mathbf{q}$,

$$\int_\Gamma \nabla_\Gamma \cdot \mathbf{q} \, d\Gamma = \int_\Gamma \kappa \, \check{\mathbf{n}} \cdot \mathbf{q} \, d\Gamma + \int_{\partial\Gamma} \check{\boldsymbol{\nu}} \cdot \mathbf{q} \, d\partial\Gamma \tag{22}$$

where $\check{\mathbf{n}}$ is the unit vector normal to Γ and $\boldsymbol{\nu}$ is the unit vector tangent to Γ and normal to $\partial\Gamma$. As a corollary, we have that the integral of the surface divergence of a purely tangential field on a closed surface is zero. The detailed proof is found in Buscaglia and Ausas (2011)

Applying (22) with $\mathbf{q} = \gamma \mathbf{v}$ to (20), since

$$\gamma \nabla \cdot \widehat{\mathbf{v}} = \nabla \cdot (\widehat{\gamma} \, \widehat{\mathbf{v}}) - \nabla \widehat{\gamma} \cdot \widehat{\mathbf{v}} = \nabla_\Gamma \cdot (\gamma \mathbf{v}) - \nabla_\Gamma \gamma \cdot \mathbf{v} \tag{23}$$

gives

$$d\mathcal{E}(\Gamma; \mathbf{v}) = -\mathcal{P}_\Gamma(\mathbf{v}) = \int_\Gamma (\gamma \, \kappa \, \check{\mathbf{n}} - \nabla_\Gamma \, \gamma) \cdot \mathbf{v} \, d\Gamma + \int_{\partial\Gamma} \gamma \, \check{\boldsymbol{\nu}} \cdot \mathbf{v} \, d\partial\Gamma \tag{24}$$

An approach proposed by Bänsch (2001), computes $\mathcal{P}_\Gamma(\mathbf{w})$ as follows

$$\mathcal{P}_\Gamma(\mathbf{w}) = -\int_\Gamma \gamma \, \mathbf{P} : \nabla \mathbf{w} \, d\Gamma \tag{25}$$

which comes from (20), since

$$\nabla_\Gamma \cdot \mathbf{v} = \nabla \cdot \widehat{\mathbf{v}} = \text{trace}(\nabla \mathbf{v} \cdot \mathbf{P}) = \mathbf{P} : \nabla \mathbf{v} = (\mathbb{I} - \check{\mathbf{n}} \otimes \check{\mathbf{n}}) : \nabla \mathbf{v} \tag{26}$$

2.2 Virtual work in the presence of contact lines

Now we consider that the surface Γ touches the boundary $\partial\Omega$ splitting it into a part that is in contact with one fluid (Γ_{s+}) and a part that is in contact with the other fluid (Γ_{s-}). The boundary of Γ, denoted by $\partial\Gamma$, is a curve on $\partial\Omega$.

The changes in energy at the boundary $\partial\Omega$ when Γ moves must be considered, so that the total interface energy analogous to (5) is

$$\mathcal{E}(\Gamma) = \int_\Gamma \gamma \, d\Gamma + \int_{\Gamma_{s+}} \gamma_{s+} \, d\Gamma_s + \int_{\Gamma_{s-}} \gamma_{s-} \, d\Gamma_s \tag{27}$$

where γ_{s+} and γ_{s-} denote the energy densities of the interfaces solid/fluid A and solid/fluid B, respectively. Let us denote by $\mathcal{E}_s(\Gamma)$ the sum of the second and third terms in the definition of $\mathcal{E}$ above, i.e.

$$\mathcal{E}_s(\Gamma) = \int_{\Gamma_{s+}} \gamma_{s+} \, d\Gamma_s + \int_{\Gamma_{s-}} \gamma_{s-} \, d\Gamma_s. \tag{28}$$

It can be proved that the variations of $\mathcal{E}_s(\Gamma)$ are given by

$$d\mathcal{E}_s(\Gamma; \mathbf{w}) = \int_{\partial\Gamma_{s+}=\partial\Gamma} (\gamma_{s-} - \gamma_{s+}) \, \check{\boldsymbol{\nu}}_s \cdot \mathbf{w} \, d\partial\Gamma \tag{29}$$

where $\check{\boldsymbol{\nu}}_s$ is the unit vector tangential to the solid boundary and normal to the contact line (see Figure 1).

In the shape derivative above the fluid must slip on the surface for the contact line to move. This is contrary to the no–slip behavior that is observed away from contact lines. It would also
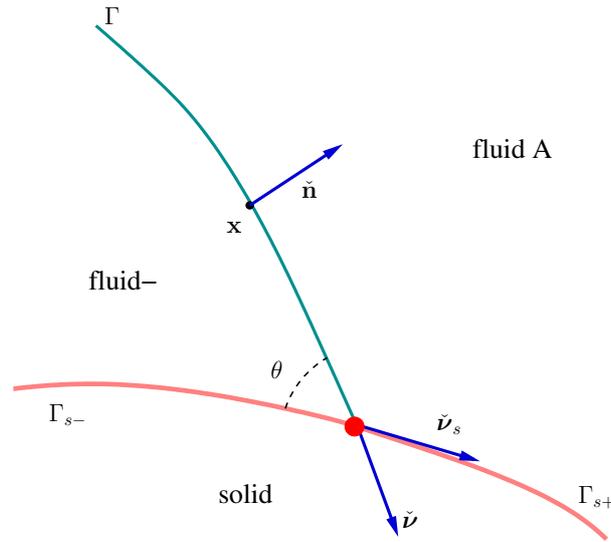
Figure 1: Detail of the geometrical definitions near the triple contact. The contact line $\partial\Gamma$ cuts the plane of the figure perpendicularly at the red dot.

be unphysical to assume a free–slip boundary, thus it is usual to add a Navier–type slip law at $\partial\Omega$, corresponding to a tangential force $\mathbf{t}$ proportional to $\mathbf{u}$ (i.e.; $\mathbf{t} = -\beta\,\mathbf{u}$).

The corresponding virtual dissipation is, thus,

$$\mathcal{P}_{\partial\Omega}(\mathbf{w}) = -\int_{\partial\Omega} \beta\,\mathbf{u}\cdot\mathbf{w}\,d\partial\Omega. \tag{30}$$

Since slip is believed to take place only at molecular distances from the contact line, β is essentially $+\infty$ everywhere except in a very small vicinity of $\partial\Gamma$. In simulations, the size of this vicinity is taken as the mesh size (Renardy et al., 2001). A recent discussion of slip models and their impact on the motion of the interface Γ can be found in Ren and Weinan (2007). In the numerical examples to be shown later, however, a constant value of β was adopted to simplify the presentation. Though some dissipation has been added at $\partial\Omega$ through the Navier term, none has been incorporated at Γ or at $\partial\Gamma$ (the first and second integrals above are "elastic"). The lack of a concentrated dissipation at $\partial\Gamma$ has very important mechanical consequences, as detailed next. At this point, the problem to be solved is

Let $(\mathbf{u}, p) \in W \times Q$ satisfy

$$\int_{\Omega} 2\mu\,D\mathbf{u} : D\mathbf{w}\,d\Omega - \int_{\Omega} p\,\nabla\cdot\mathbf{w}\,d\Omega = \int_{\Gamma} \gamma\,(\mathbb{I} - \check{\mathbf{n}}\otimes\check{\mathbf{n}}) : \nabla\mathbf{w}\,d\Gamma -$$

$$-\int_{\partial\Gamma} (\gamma_{s-} - \gamma_{s+})\,\check{\boldsymbol{\nu}}_s\cdot\mathbf{w}\,d\partial\Gamma - \int_{\partial\Omega} \beta\,\mathbf{u}\cdot\mathbf{w}\,d\partial\Omega \tag{31}$$

for all $\mathbf{w} \in W$, and let $\mathbf{u}$ also satisfy $\nabla\cdot\mathbf{u} = 0$. In (31), as before, $\check{\boldsymbol{\nu}}_s$ is the unit vector tangential to the solid boundary and normal to the contact line. Now, based on (31) (i.e., in the absence of a localized virtual dissipation) it is possible to obtain

$$\check{\boldsymbol{\nu}}\cdot\check{\boldsymbol{\nu}}_s = \cos\theta = \frac{\gamma_{s+} - \gamma_{s-}}{\gamma} \tag{32}$$

Let

$$M = \frac{\gamma_{s+} - \gamma_{s-}}{\gamma} \tag{33}$$

If $|M| \leq 1$ define the **static contact angle** as

$$\theta_S = \text{arc cos } M \qquad (\text{i.e. } \gamma \cos \theta_S = \gamma_{s+} - \gamma_{s-}) \tag{34}$$

if not, $\theta_S = 0$. This latter case is perfectly physical and corresponds to the **total wetting** case, in which one of the liquids spreads completely on the solid, displacing the other. The dynamics of the spreading is limited by dissipative processes near the contact line, and can be very slow.

By direct inspection of (32) we conclude the following:

- If $|M| \leq 1$, the interface shapes Γ in the variational formulation (31) make an angle $\theta = \theta_S$ with the solid boundary at all times. There is no "dynamic" contact angle different from the static one, since

$$\gamma \left(\cos \theta - \cos \theta_S \right) \check{\boldsymbol{\nu}}_s = 0 \tag{35}$$

- If $|M| > 1$, on the other hand, the mathematical problem is not well posed.

This shows that the basic model above is contradictory with experiments, since the angle θ is known to depend on whether the contact line is advancing or receding, and on its velocity (see e.g. Hocking (1981); Haley and Miksis (1991) an references therein). The inability of the model to cope with the total–wetting situation is also a drawback. Numerical implementations yield solutions strongly dependent on the mesh, as recently shown by Afkhami et al. (2009), Weinstein and Pismen (2008) and Spelt (2005).

Virtual dissipation at the contact line

One possible (numerical) cure to the the unphysical behaviors previously mentioned is to add a localized dissipation of the form

$$\mathcal{P}_{\partial\Gamma,\text{diss}}(\mathbf{w}) = \int_{\partial\Gamma} \mathbf{f}_{\text{diss}} \cdot \mathbf{w} \, d\partial\Gamma \tag{36}$$

to the right-hand side of the variational formulation (31). Implying that the flow will adjust so that

$$\mathbf{f}_{\text{diss}} = F \, \check{\boldsymbol{\nu}}_s \tag{37}$$

where F is called *out-of-balance interfacial tension*

$$F = \gamma(\cos \theta_S - \cos \theta). \tag{38}$$

For example, if the adopted model reads

$$\mathbf{f}_{\text{diss}} = - \zeta \, \mathbf{u} \tag{39}$$

with ζ a parameter that may depend on the flow variables. *A fortiori* this implies that the velocity will be parallel to $\check{\boldsymbol{\nu}}_s$ and thus perpendicular to the contact line; i.e.,

$$\mathbf{u}(\mathbf{x}, t) = V(\mathbf{x}, t) \, \check{\boldsymbol{\nu}}_s(\mathbf{x}, t) \qquad \text{for } \mathbf{x} \in \partial\Gamma(t) \tag{40}$$

3   NUMERICAL EXAMPLES

3.1   Thermocapillary migration of a droplet

Let $W_h \subset W$ be the standard $\mathbb{P}_1$ element for velocity, and let $Q_h \subset Q$ be the discrete space for pressure proposed by Ausas *et al* Ausas et al. (2010a). The stabilized discrete variational formulation adopted reads: *Find* $(\mathbf{u}_h, p_h) \in W_h \times Q_h$ *such that*

$$\int_\Omega 2\mu \, D\mathbf{u}_h : D\mathbf{w}_h \, d\Omega - \int_\Omega p_h \, \nabla \cdot \mathbf{w}_h \, d\Omega \;\; = \;\; -\int_{\Gamma_h} \gamma \, \mathbf{P} : \nabla \mathbf{w}_h \, d\Gamma \tag{41}$$

$$\int_\Omega q_h \, \nabla \cdot \mathbf{u}_h \, d\Omega + \int_{\Omega'} \tau_h \, \nabla p_h \cdot \nabla q_h \, d\Omega \;\; = \;\; 0 \tag{42}$$

for all $(\mathbf{w}_h, q_h) \in W_h \times Q_h$, where $\Omega' = \Omega \setminus \Gamma = \Omega^+ \cup \Omega^-$ and $\tau_h = c_\tau \frac{h^2}{\mu}$ (Hughes et al., 1986; Codina, 2001; Codina et al., 2001), with $c_\tau = \frac{1}{40}$. As an additional approximation, Γ_h is defined as the zero–level set of a piecewise–linear function ϕ_h. The integral over Γ_h is performed exactly, with γ assumed constant in each element. As done in Ausas et al. (2010a), the stabilization is turned off ($\tau_h = 0$) in the elements cut by the interface.

We aim to show here, by means of a numerical example, that the formulation (41)–(42) accurately accounts for both the surface tension force and the Marangoni force. Remember that the Marangoni force equals $\nabla_\Gamma \gamma$, and induces tangential motion of the fluid at the interface. Physically, non–uniformities of γ can result from a non–uniformly distributed surfactant or due, for instance, to temperature gradients (the surface tension coefficient γ decreases with increasing temperature).

The example we have chosen is the migration of an immiscible spherical droplet in an unbounded domain (in the absence of gravity) with a linear distribution for γ,

$$\gamma(\mathbf{x}) = \gamma_0 - \dot{\gamma} \, x, \qquad\qquad \dot{\gamma} > 0 \tag{43}$$

This problem has been thoroughly studied both theoretically and experimentally in the past (see e.g. Young et al. (1959); Balasubramaniam and A-T. (1987) and references therein). A sketch of the geometry and choice of coordinates can be found in Figure 2. The corresponding differential equations and interface conditions are

$$-\mu \nabla^2 \mathbf{u} + \nabla p = 0 \quad \text{on } \Omega' \tag{44}$$

$$\nabla \cdot \mathbf{u} = 0 \quad \text{on } \Omega \tag{45}$$

$$[\![\boldsymbol{\sigma}]\!] \cdot \check{\mathbf{n}} = -\gamma \, \kappa \, \check{\mathbf{n}} + \nabla_\Gamma \gamma \quad \text{on } \Gamma \tag{46}$$

to be solved subject to the far–field conditions

$$\mathbf{u}(\mathbf{x} \to \infty) = \mathbf{0} \qquad\qquad p(\mathbf{x} \to \infty) = p_\infty \tag{47}$$

The exact solution to (44)–(47) exhibits a motion of the droplet along $+x$, with velocity

$$U = \frac{2}{15} \frac{\dot{\gamma} \, R}{\mu} \tag{48}$$

which drives the interface towards regions with lower values of γ, thus reducing its energy. Let us define

$$\mathbf{v} = \mathbf{u} - U \, \check{\mathbf{i}} \tag{49}$$
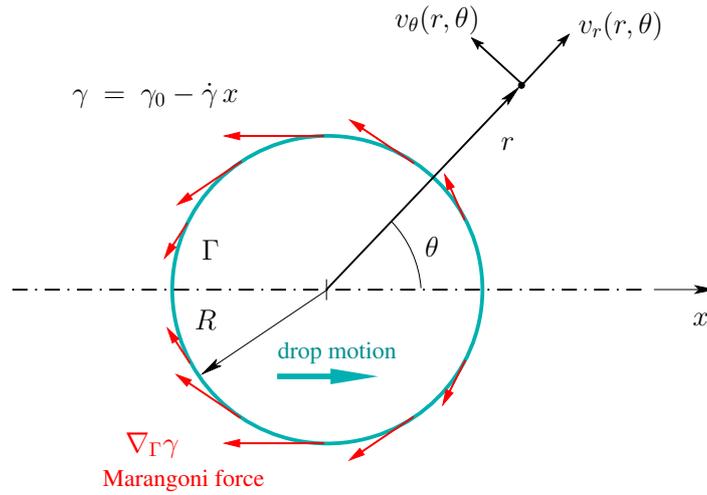
Figure 2: Problem setting for the thermocapillary motion of a spherical droplet.

with $\check{\mathbf{i}}$ the unit vector along x. Then, the radial and tangential components of $\mathbf{v}$, and the pressure, can be shown to be

$$r > R \qquad \begin{cases} v_r^+ = -U \cos\theta \left(1 - \frac{R^3}{r^3}\right) \\ v_\theta^+ = U \sin\theta \left(1 + \frac{R^3}{2\,r^3}\right) \\ p^+ = p_\infty \end{cases} \tag{50}$$

$$r < R \qquad \begin{cases} v_r^- = \frac{3}{2}U \cos\theta \left(1 - \frac{r^2}{R^2}\right) \\ v_\theta^- = 3\,U \sin\theta \left(\frac{r^2}{R^2} - \frac{1}{2}\right) \\ p^- = p_\infty + \frac{2}{R}(\gamma_0 - \dot{\gamma}\,r \cos\theta) \end{cases} \tag{51}$$

Notice that $\mathbf{v}$ is purely tangential at the fluid interface, i.e., the radial component is zero ($v_r^-(r = R, \theta) = v_r^+(r = R, \theta) = 0$). This implies that the shape does not change with time and thus the droplet moves at a constant velocity.

For the numerical simulations, we solve (41)–(42) using an axisymmetric 2D code, so that the horizontal coordinate is x and the vertical coordinate y is in fact the distance from the x-axis. Once $\mathbf{u}_h$ is obtained, we compute $\mathbf{v}_h = \mathbf{u}_h - U\,\check{\mathbf{i}}$. The computational domain is taken as $0 < x < 12R$, $0 \le y < 4R$, with $R = 0.25$. It is discretized with 60000 linear triangular elements which do not follow Γ. The approximate interface Γ_h is obtained as the zero-level set of the nodal signed distances to Γ and cuts the elements arbitrarily. We consider viscosities $\mu_A = \mu_B = 1$ and $p_\infty = 0$, and surface tension parameters $\gamma_0 = 3$ and $\dot{\gamma} = 1$. The numerical results obtained match quite well the exact solution, as shown in Figure 3 where the numerical and exact $\mathbf{v}$-velocity contours are shown, respectively, above and below the x-axis. The velocity vectors, which are painted with the pressure field, are tangent to the droplet interface. We also show in Figure 4 the normal and tangential components of the velocity field $\mathbf{v}_h$ on Γ, as a function of the angle θ, and compare them with the exact values $v_r(r = R, \theta) = 0$ and $v_t(r = R, \theta) = 3/2\,U \sin\theta$. As can be noticed in the figure, there is good agreement between them showing that the Marangoni force is accurately accounted for.

A cross-section of the pressure field along the x-axis is plotted in Figure 5. The pressure jump across Γ depends on the position, since $[\![p]\!] = 2\gamma/R$ and γ depends on x. This is captured
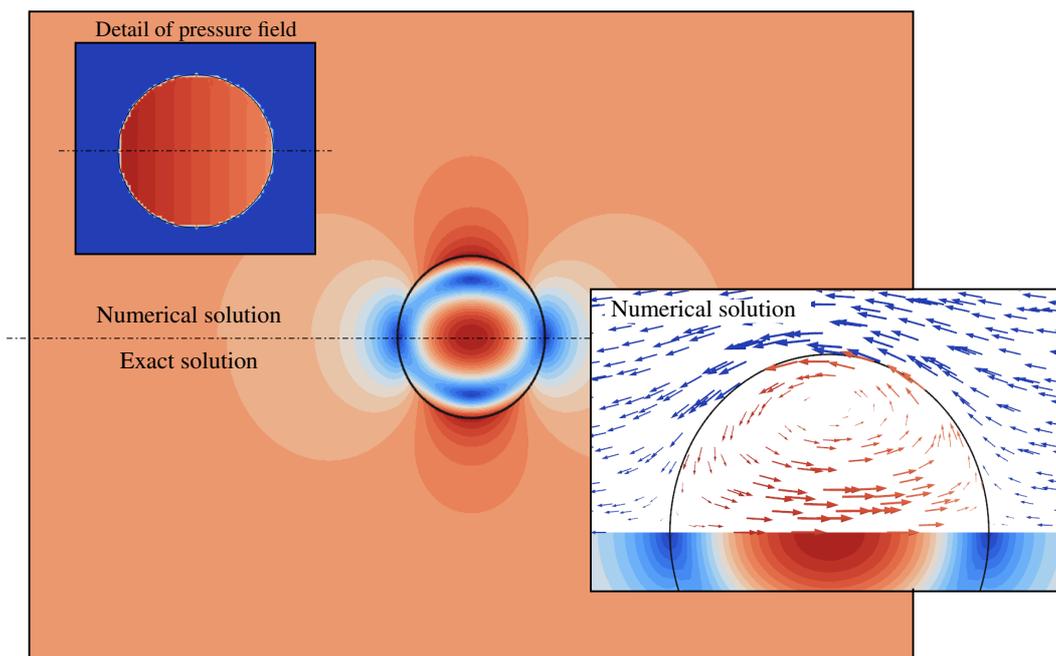
Figure 3: Comparison of the velocity magnitude and pressure fields for the thermocapillary migration of a droplet. The solution above the symmetry line corresponds to the numerical results and the one underneath is the exact solution. The maximum in the colour scale of the velocity field (red) corresponds to 0.05 and the minimum (blue) to 0. The velocity vectors are shown in the insert, with the colors corresponding to the pressure field.

by the method, as can be inferred from the left ($[\![p]\!]_\ell$) and right ($[\![p]\!]_r$) pressure jumps shown in the figure, which agree well with the exact values.

We also report an assessment of the numerical method in the three dimensional case. A mesh with $1,110,000$ linear tetrahedral elements is used to discretize the computational domain $[0,3R] \times [0,2R] \times [0,2R]$. As before, the mesh does not conform to the interface. The results are in good agreement with the axisymmetrical ones, as shown in Figure 6, where the velocity field $\mathbf{v}_h$ and its streamlines are plotted. Notice in the insert the field $\mathbf{u}_h$, the direct result of the code.

3.2 Spreading droplets

Level–set finite element method

In the previous example the interface was fixed. Now, we adopt the same stabilized finite element method of the previous section, but considering the temporal evolution of the interface. The time step size is denoted by Δt, and all variables are assumed known at time t_n, so that the unknowns correspond to time t_{n+1}. The level–set function ϕ_h belongs to the space Φ_h, which is taken as the standard $\mathbb{P}_1$ space. The time–step index appears as a supre–index. The discrete problem at each time step thus reads:

Find $(\mathbf{u}_h^{n+1}, p_h^{n+1}, \phi_h^{n+1}) \in W_h \times Q_h \times \Phi_h$ *such that*
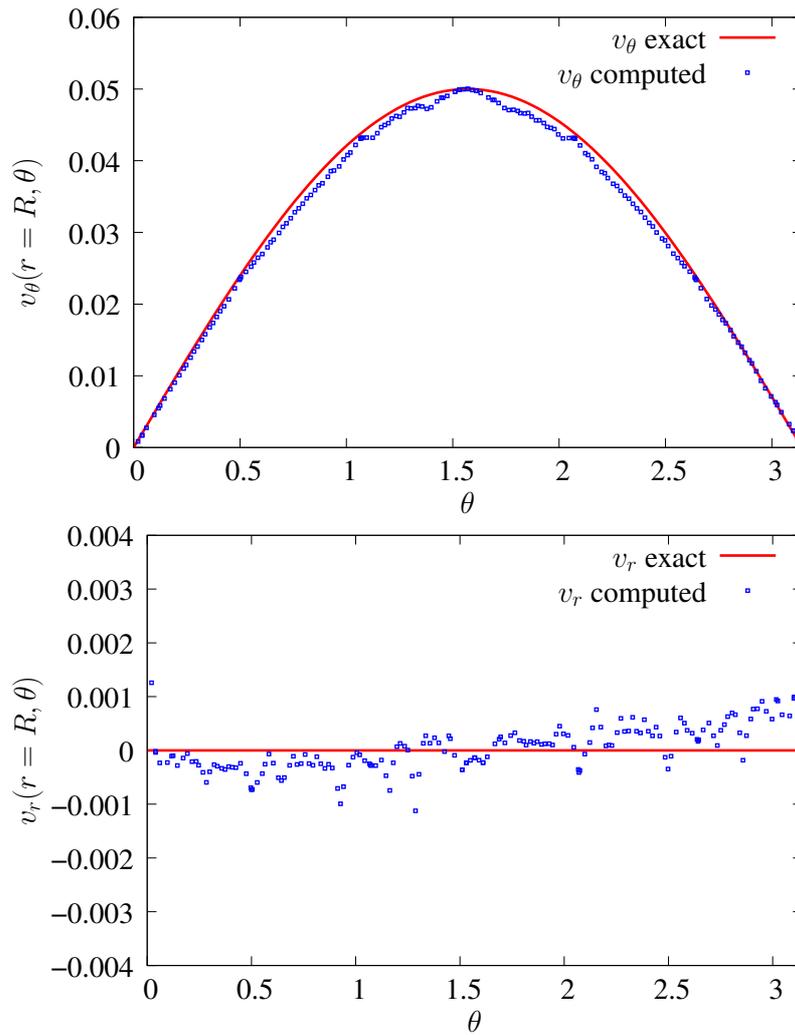
Figure 4: Comparison of the numerical and exact normal and tangential components of the velocity field for the thermocapillary migration of a droplet.
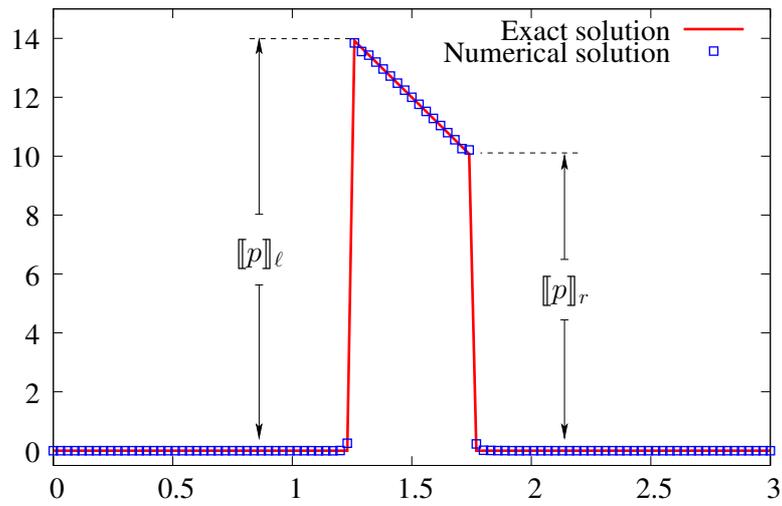
Figure 5: Comparison of the numerical and exact pressure fields along the symmetry axis for the thermocapillary migration of a droplet.
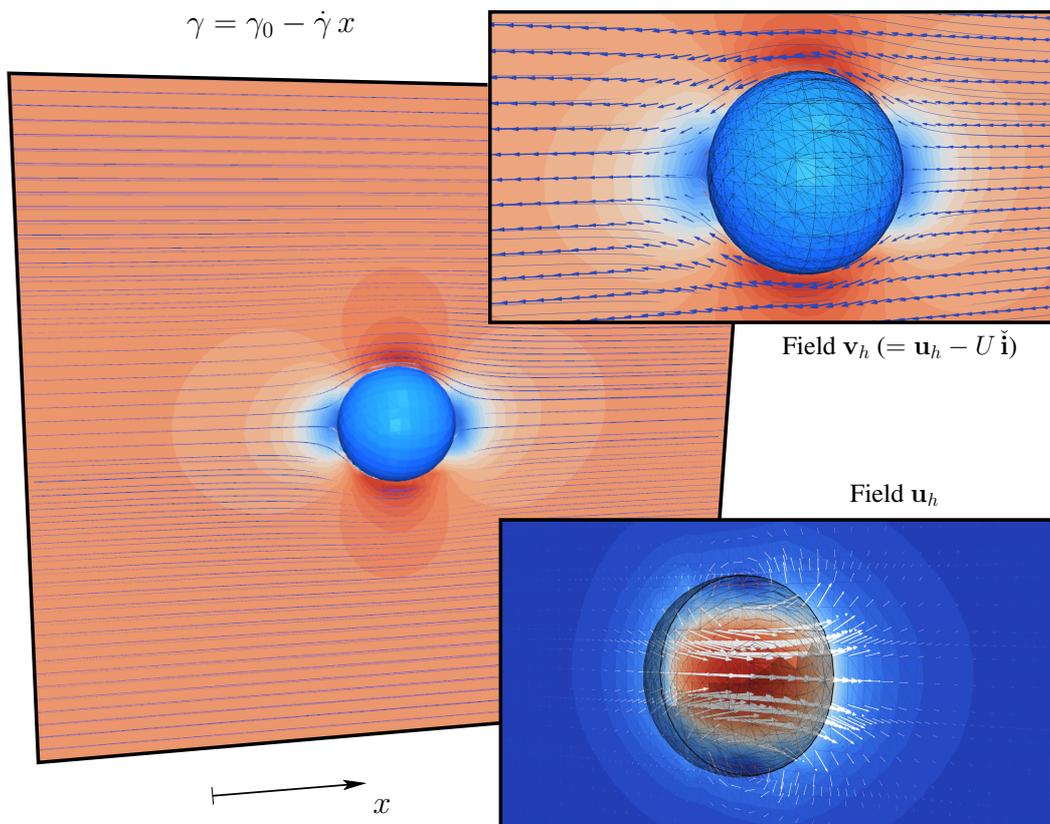
Figure 6: Velocity field for the three dimensional simulation of the thermocapillary migration of a droplet. To provide an idea of the mesh size the reconstructed facets of Γ_h are drawn.

$$\int_\Omega 2\mu\, D\mathbf{u}_h^{n+1} : D\mathbf{w}_h\, d\Omega - \int_\Omega p_h^{n+1} \nabla \cdot \mathbf{w}_h\, d\Omega \;=\; \int_{\Gamma_h^{n+1}} \gamma\, \mathbf{P}^{n+1} : \nabla \mathbf{w}_h\, d\Gamma -$$

$$- \int_{\partial\Gamma_h^{n+1}} \left(\gamma\, M \,+\, \zeta\, \check{\boldsymbol{\nu}}_s \cdot \mathbf{u}_h^{n+1} \right) \check{\boldsymbol{\nu}}_s \cdot \mathbf{w}_h\, d\partial\Gamma \;-\; \int_{\partial\Omega} \beta\, \mathbf{u}_h^{n+1} \cdot \mathbf{w}_h\, d\partial\Omega \quad (52)$$

$$\int_\Omega q_h\, \nabla \cdot \mathbf{u}_h^{n+1}\, d\Omega + \int_{\Omega'} \tau_h\, \nabla p_h^{n+1} \cdot \nabla q_h\, d\Omega \;=\; 0 \tag{53}$$

$$\int_\Omega \left[\frac{\phi_h^{n+1} - \phi_h^n}{\Delta t} + \mathbf{u}_h^{n+1} \cdot \nabla \phi_h^{n+1} \right] \left[\psi_h + \tilde{\tau}_h\, \mathbf{u}_h^{n+1} \cdot \nabla \psi_h \right]\, d\Omega \;=\; 0 \tag{54}$$

for all $(\mathbf{w}_h, q_h, \psi_h) \,\in\, W_h \times Q_h \times \Phi_h$. Above, $\tilde{\tau}_h = \tilde{c}\, \frac{h}{\|\mathbf{u}_h^n\|}$ and $\tilde{c} = 0.5$, corresponding to a SUPG treatment of advection. Notice that

$$\Gamma_h^{n+1} = \{\mathbf{x} \,\in\, \Omega \mid \phi_h^{n+1}(\mathbf{x}) = 0\} \tag{55}$$

and

$$\mathbf{P}^{n+1} = \mathbb{I} - \check{\mathbf{n}} \otimes \check{\mathbf{n}} \qquad \text{with} \qquad \check{\mathbf{n}} = \frac{\nabla \phi_h^{n+1}}{\|\nabla \phi_h^{n+1}\|} \tag{56}$$

The level set is periodically reinitialized using a geometrical mass–conserving technique (Mut et al., 2006; Ausas et al., 2010b).

Let us begin by assessing the finite element formulation (52)–(54) in the case without contact line dissipation ($F = 0$, i.e., $\zeta = 0$). The parameters are set to

$$\theta_S = 45°, \;\; \mu_A = 10^{-5}, \;\; \mu_B = 0.2 \times 10^{-6}, \;\; \gamma = 0.075, \;\; \beta = 10^{-5}, \;\; \Delta t = 2 \times 10^{-7}$$

and the problem is considered two-dimensional (not axisymmetric).

The initial condition corresponds to an interface that forms an angle $\theta(t = 0) = 90°$. The numerically–obtained interfaces at later times are shown in Figure 7. On the left side of the figure the interface is plotted, while the detail of the contact point (on the right) shows that the interface assumes the static angle near the wall from the very beginning. The last frame corresponds to the steady state shape of the droplet. A snapshot of the field variables at time $t = 8 \times 10^{-6}$ is shown in Figure 8. The previous simulation was run on a mesh with typical mesh size $h = 1.3 \times 10^{-3}$.

In Figure 9 we plot the contact angle as a function of time. It is clear that if $\zeta = 0$ the numerical simulation yields contact angles that are at all times equal to the static angle. The numerical contact angle was measured as the angle of the zero–level set of ϕ_h with the boundary, and exhibits some oscillations that result from the reinitialization and from the passage of the interface from one element to another.

In the same figure we also show the numerically–obtained angles for non–zero local contact–line dissipation. To simplify the presentation, three *constant* values were chosen: $\zeta = 10^{-5}$, 10^{-4} and 5×10^{-3}. In this case *dynamic* contact angles are observed, that relax towards θ_S as time evolves. No attempt has been made to tune ζ (probably as a function of $\mathbf{u}$) so as to fit some set of experimental data, since the numerical tests are oriented towards a critical assessment of the variational formulation.

It should be noticed that a length scale ℓ_β appears as a result of the Navier's boundary condition,

$$\ell_\beta = \frac{\mu_A}{\beta},$$
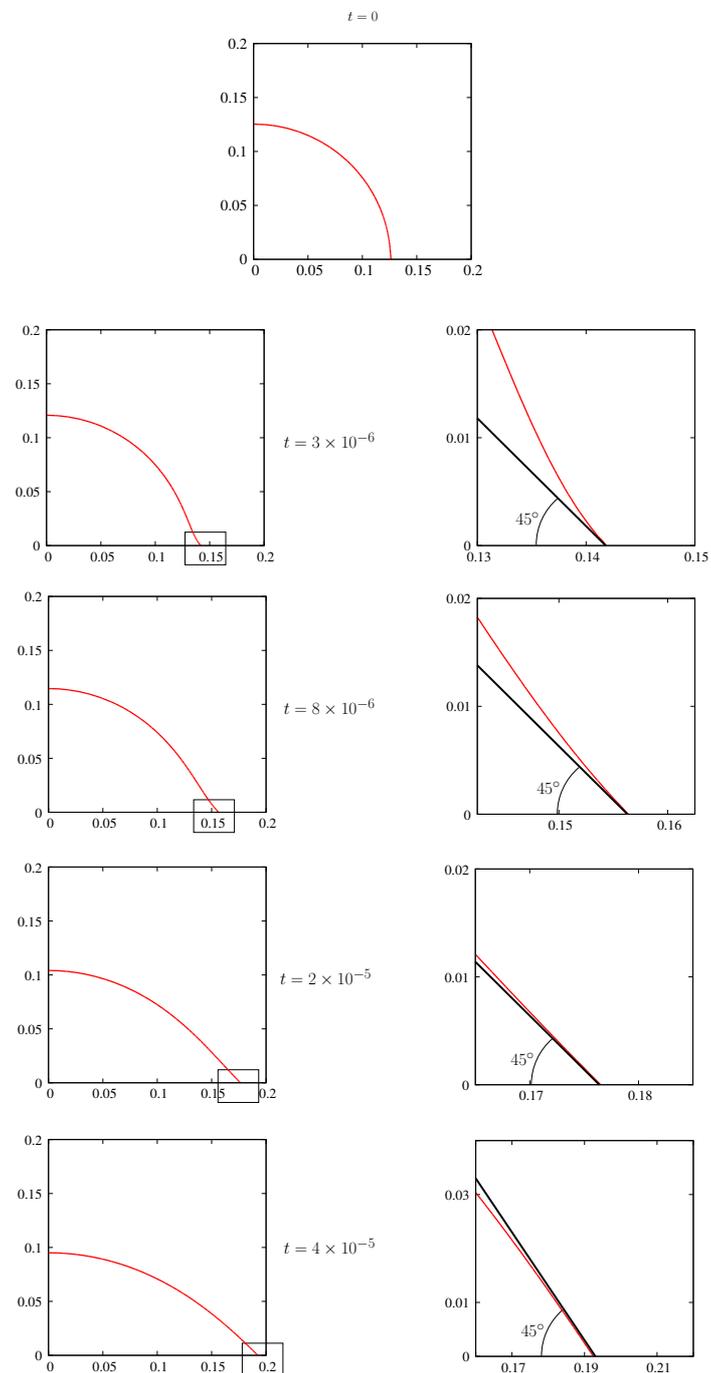
Figure 7: Interface at different times for the spreading droplet. For each time in the right column, a detail of the interface and a straight line with $45°$ inclination is drawn.
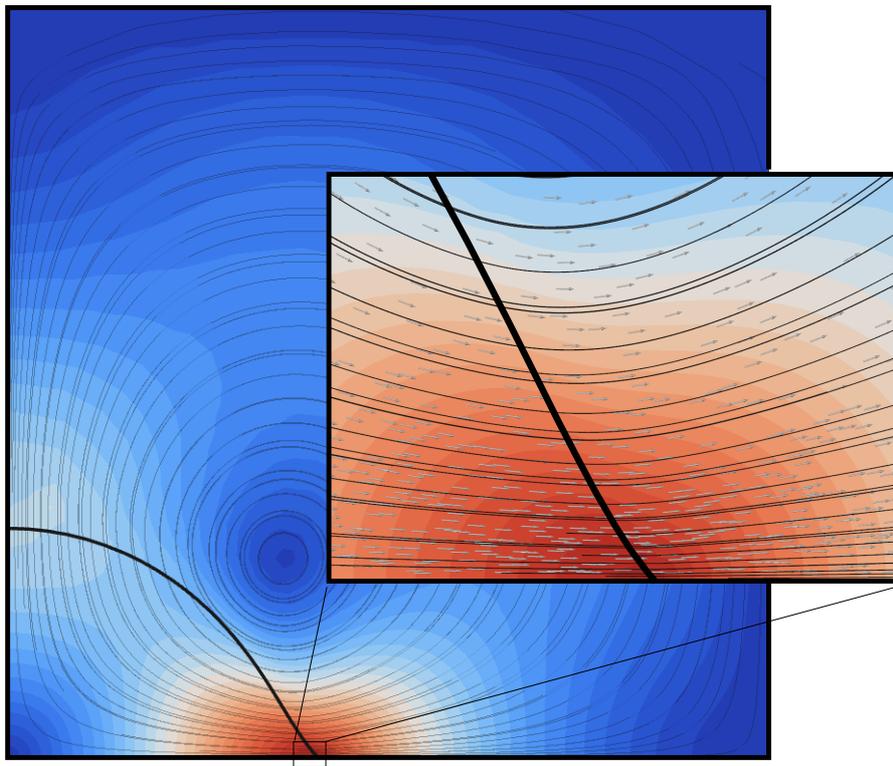
Figure 8: Snapshot of the flow field at $t = 8 \times 10^{-6}$ for the case of Figure 7. Velocity magnitude contours, streamlines and normalized velocity vectors. Slip coefficient β equal to 10^{-5} (corresponding to a slip length *well resolved by the mesh*) and without considering local dissipation ($\zeta = 0$). The maximum in the colour scale (red) corresponds to 2673 and the minimum (blue) to 0.
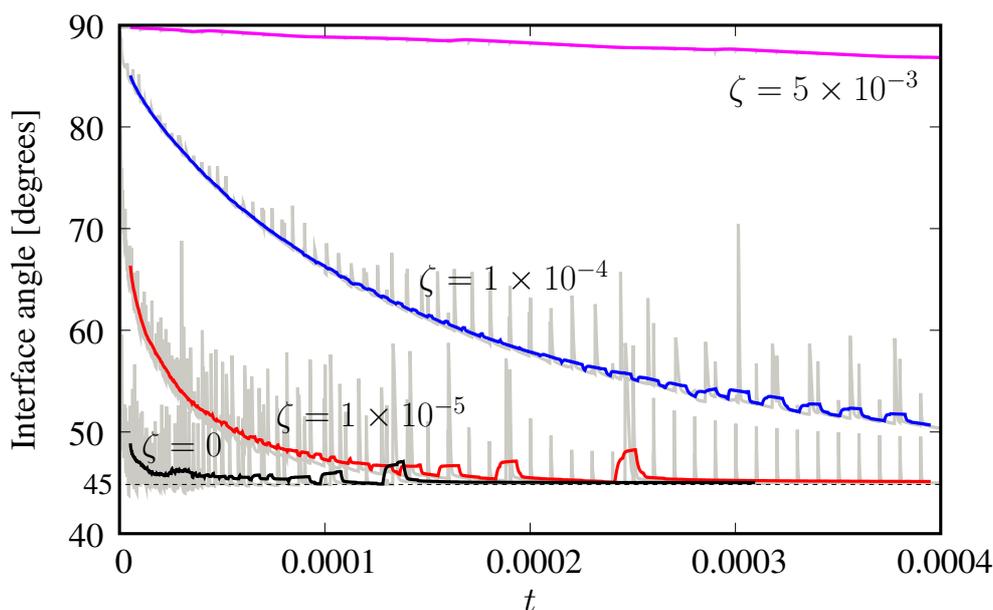
Figure 9: Measured angle as a function of time for the spreading droplet with $\theta_S = 45°$ and different values for the constant ζ.

which in the case discussed above takes the value $\ell_\beta = 1$, so that $h \ll \ell_\beta$. In general, simulations are not able to resolve the slip length, making it important to assess the numerical method for larger values of β and coarser meshes.

Considering thus $\beta = 2 \times 10^{-2}$ (i.e.; $\ell_\beta = 5 \times 10^{-4}$), the code was run both on the previous mesh ($h = 1.3 \times 10^{-3}$) and on a coarser one ($h = 5 \times 10^{-3}$). The numerically obtained angles are shown in Figure 10, both for $\zeta = 0$ and $\zeta = 5 \times 10^{-3}$. In agreement with Ganesan and Tobiska (2009), for these underresolved cases the contact angle seems to be different from θ_S even with $\zeta = 0$. Notice however that this "dynamics" is strongly dependent on the mesh and thus a numerical artifact. With $\zeta = 5 \times 10^{-3}$, on the other hand, the dynamics of the contact angle is less mesh–dependent and thus indicative of some true underlying dynamics. The same strong mesh sensitivity of the case $\zeta = 0$ is observed for the interface position (see Figure 11). Though the difficulty persists with $\zeta = 5 \times 10^{-3}$, it is less pronounced, thus showing the numerical advantage of adding a local dissipation at the contact line.

In Figures 12 and 13 we show the flow variables corresponding to underresolved simulations $\beta = 2 \times 10^{-2}$ on the fine mesh ($h = 1.3 \times 10^{-3}$), for $\zeta = 0$ and $\zeta = 5 \times 10^{-3}$, respectively. The instants ($t = 7.5 \times 10^{-5}$ and $t = 3.1 \times 10^{-3}$) were chosen so that the contact line is near the position $x = 0.15$, which is also the case in Figure 8 ($t = 8 \times 10^{-6}$).

As additional illustration, let us show that simulating the case of total wetting ($M > 1$) is also possible with this formulation. In Figure 14 we show the evolution of a 2D droplet with a spreading parameter $M = 2$. In this case the droplet does not reach a steady state but continues spreading at a monotonously decreasing speed. Another $M = 2$ case is reported in Figure 15. This case is three–dimensional, with an initially–prismatic shape, and was run on a mesh consisting of 480,000 tetrahedra.
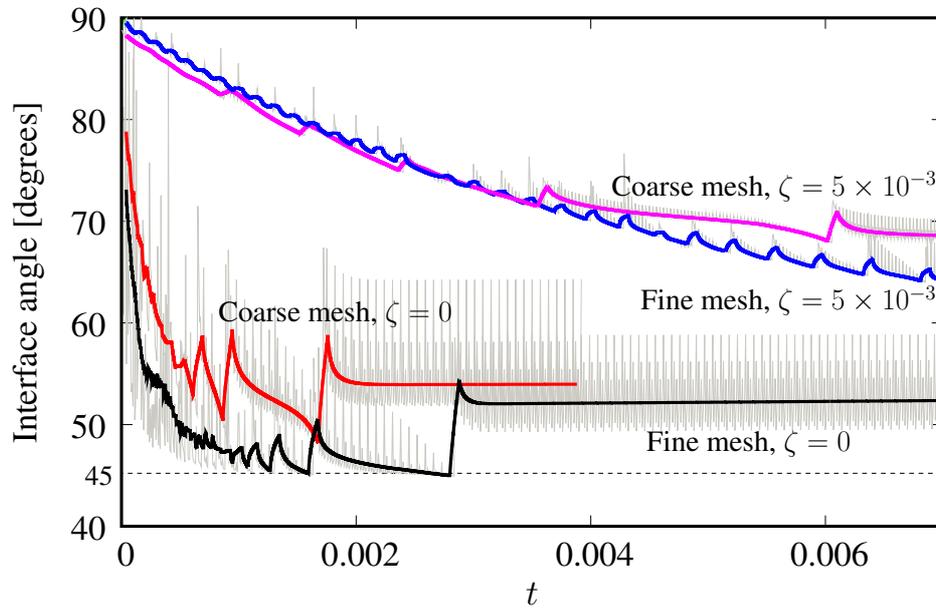
Figure 10: Interface angle at the contact point as a function of time on a coarse mesh ($h = 5.6 \times 10^{-3}$) and a fine mesh ($h = 1.3 \times 10^{-3}$). The case without local dissipation ($\zeta = 0$) and with local dissipation ($\zeta = 5 \times 10^{-3}$) are shown.
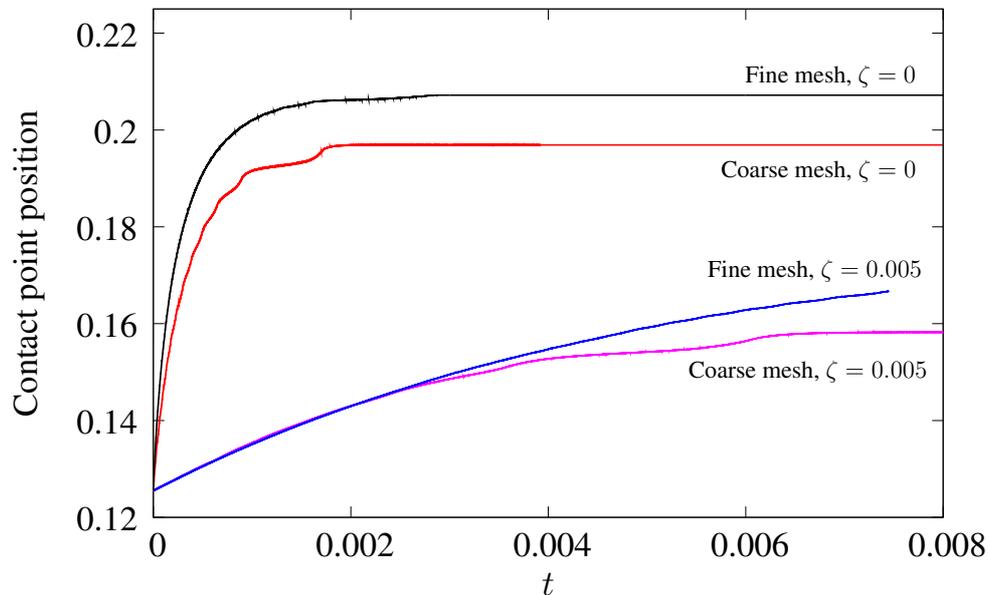
Figure 11: Comparison of the contact point position as a function of time on a coarse mesh ($h = 5.6 \times 10^{-3}$) and a fine mesh ($h = 1.3 \times 10^{-3}$). The case without local dissipation ($\zeta = 0$) and with local dissipation ($\zeta = 5 \times 10^{-3}$) are shown.
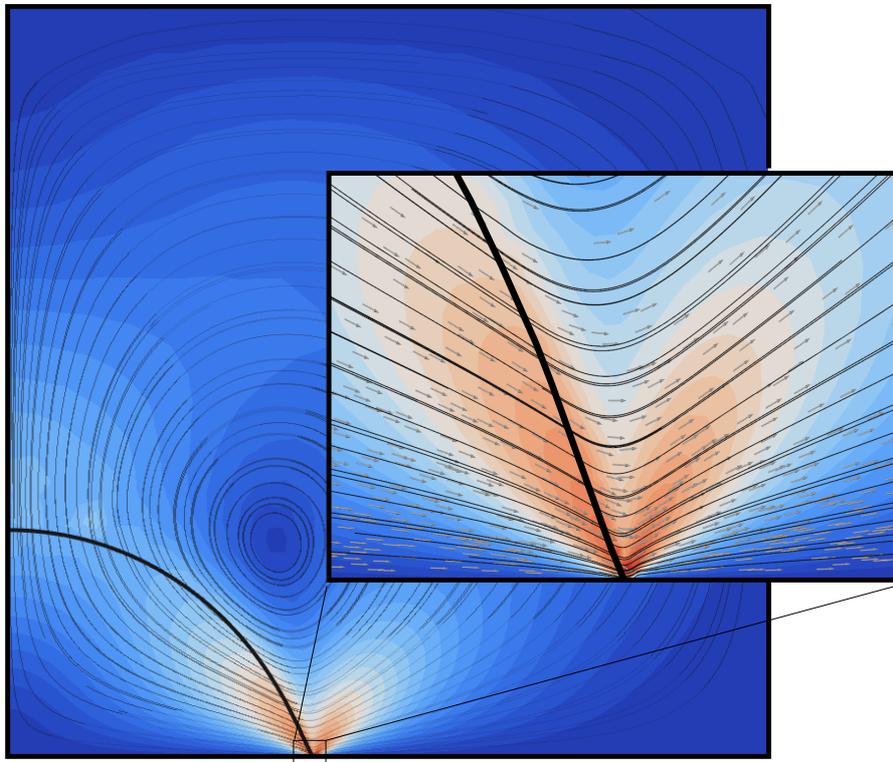
Figure 12: Velocity magnitude contours, streamlines and normalized velocity vectors. The image corresponds to time $t = 7.5 \times 10^{-5}$ and the simulation parameters are: $\beta = 2 \times 10^{-2}$, $h = 1.3 \times 10^{-3}$ and $\zeta = 0$. The maximum in the colour scale (red) corresponds to 394 and the minimum (blue) to 0.
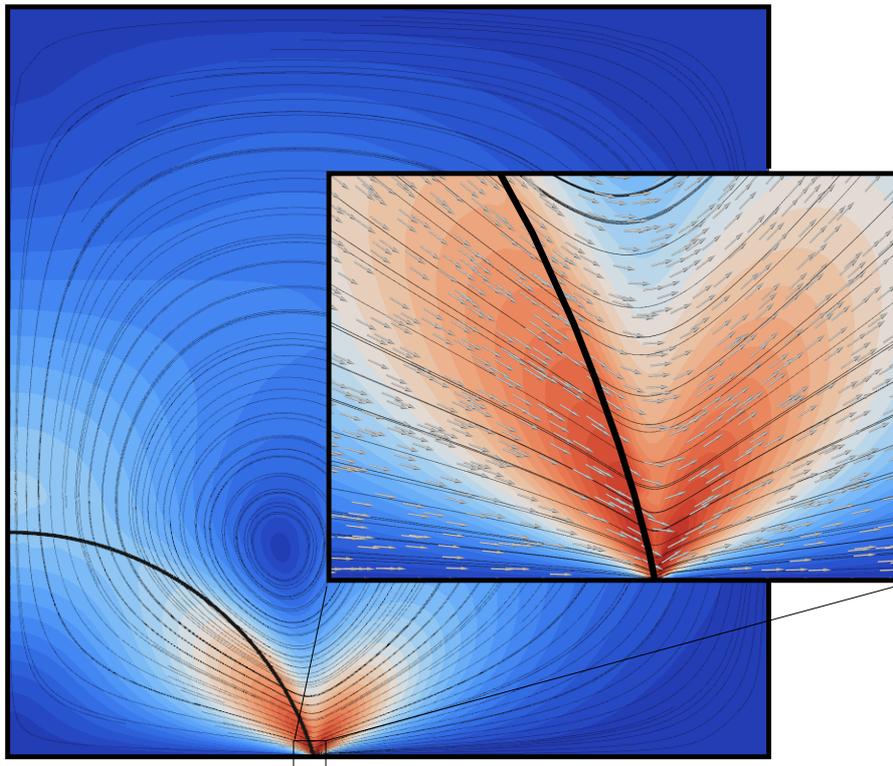
Figure 13: Velocity magnitude contours, streamlines and normalized velocity vectors. The image corresponds to time $t = 3.1 \times 10^{-3}$ and the simulation parameters are: $\beta = 2 \times 10^{-2}$, $h = 1.3 \times 10^{-3}$ and $\zeta = 5 \times 10^{-3}$. The maximum in the colour scale (red) corresponds to 7.6 and the minimum (blue) to 0.
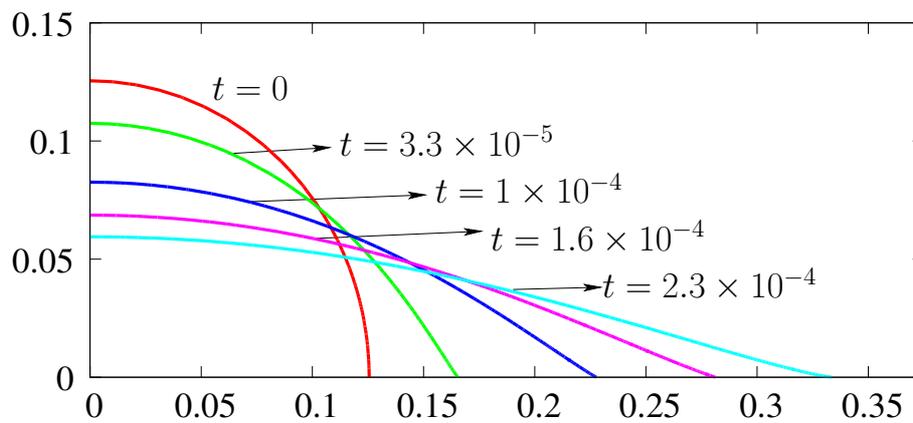
Figure 14: Interface at different times for the spreading droplet with total wetting. Simulation parameters: $M = 2$, $\beta = 10^{-5}$, $\zeta = 10^{-4}$.
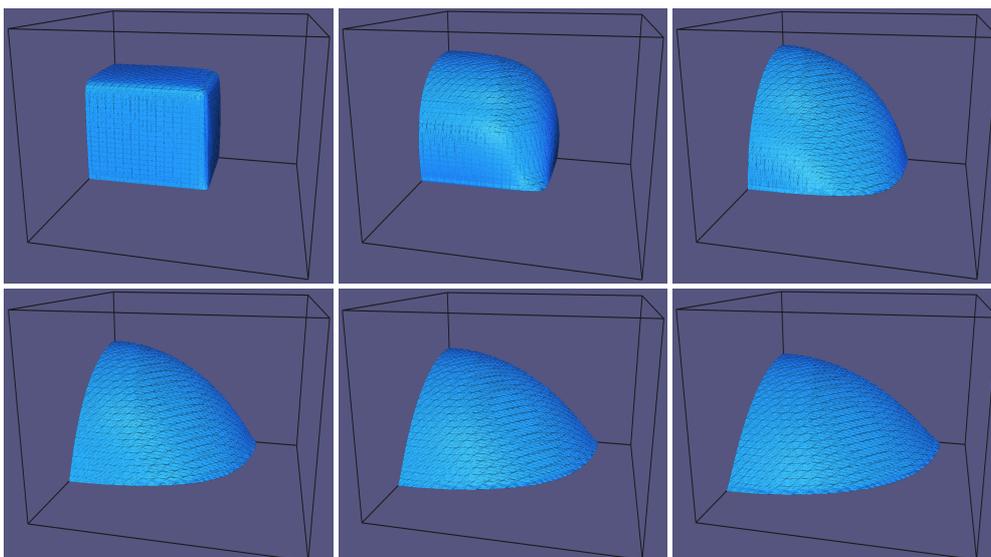
Figure 15: Interface at different times for the spreading of an initially–prismatic droplet with total wetting. The simulation parameters are: $M = 2$, $\beta = 2 \times 10^{-2}$, $\zeta = 10^{-4}$. Shown are the times $t = 0$, 2×10^{-5}, 10^{-4}, 2×10^{-4}, 3×10^{-4} and 4×10^{-4}. Prism geometry: $(-0.125, 0.125) \times (-0.175, 0.175) \times (0, 0.125)$. Symmetry used at $x = 0$ and $y = 0$.

4   FINAL REMARKS

In this article a discussion on surface tension related phenomena within the framework of variational formulations, has been presented. In this formulation, the capillary forces are derived from variations of the interfacial energy. This has been done by embedding Γ into $\mathbb{R}^3$ and adopting fixed Cartesian coordinates in 3D space thus avoiding covariant differentiation. The proposed formulation is very appealing for numerical treatment by means of the finite element method. Two illustrative numerical examples have been presented. First, the thermocapillary migration of a droplet under a constant temperature gradient was simulated. The aim in this case is to show that both, the surface tension force and the Marangoni force are accurately accounted. The numerical formulation has been assessed by means of comparing in two and three spatial dimensions the numerical results with the exact solution obtaining an excelent agreement between them. The spreading of droplets has also been studied from within the variational framework. In particular the imposition of the static contact angle and of local dissipation laws was considered. The case of total wetting, corresponding to a spreading parameter $M > 1$ was simulated both in two and three dimensions.

ACKNOWLEDGMENTS

REFERENCES

Afkhami S., Zaleski S., and Bussmann M. A mesh–dependent model for applying dynamic contact angles to VOF simulations. *J. Comput. Phys.*, 228:5370–5389, 2009.
Ausas R., Sousa F., and Buscaglia G. An improved finite element space for discontinuous

pressures. *Comput. Methods Appl. Mech. Engrg.*, 199:1019–1031, 2010a.

Ausas R.F., Buscaglia G.C., and Dari E.A. A geometric mass-preserving redistancing scheme for the level set function. *Int. J. Num. Meth. Fluids, DOI: 10.1002/fld.2227*, 2010b.

Balasubramaniam R. and A-T. C. Thermocapillary migration of droplets: An exact solution for small marangoni numbers. *Journal of Colloid and Interface Science*, 119:538–531, 1987.

Bänsch E. Finite element discretization of the Navier–Stokes equations with a free capillary surface. *Numer. Math.*, 88:203–235, 2001.

Bonito A., Nochetto R., and Pauletti S. Parametric FEM for geometric biomembranes. *Journal of Computational Physics*, 229:3171–3188, 2010.

Bonn D., Eggers J., Indekeu J., Meunier J., and Rolley E. Wetting and spreading. *Review of Modern Physics*, 81:739–767, 2009.

Breyiannis G. and Pozrikidis C. Simple Shear Flow of Suspensions of Elastic Capsules. *Theoretical and Computational Fluid Dynamics*, 13:327–347, 2000.

Buscaglia G. and Ausas R. Variational formulations for surface tension, capillarity and wetting. *Comput. Methods Appl. Mech. Engrg.*, 200(45–46):3011–3025, 2011.

Codina R. A stabilized finite element method for generalized stationary incompressible flows. *Comput. Methods Appl. Mech. Engrg*, 190:2681–2706, 2001.

Codina R., Blasco J., Buscaglia G., and Huerta A. Implementation of a stabilized finite element formulation for the incompressible Navier-Stokes equations based on a pressure gradient projection. *Int. J. Numer. Meth. in Fluids*, 37:410–444, 2001.

de Gennes P.G., Brochard-Wyart F., and Quéré D. *Capillarity and wetting phenomena. Drops, bubbles, pearls, waves*. Springer, 2004.

Dziuk G. Computational parametric Willmore flow. *Numerische Mathematik*, 111:55–80, 2008.

Fuster D., Agbaglah G., Josserand C., Popinet S., and Zaleski S. Numerical simulation of droplets, bubbles and waves: state of the art. *Fluid Dyn. Res.*, 41:065001 (24pp), 2009. http://dx.doi.org/10.1088/0169-5983/41/6/065001.

Ganesan S. and Tobiska L. A coupled arbitrary Lagrangian–Eulerian and Lagrangian method for computation of free surface flows with insoluble surfactants. *J. Comput. Phys.*, 228:2859–2873, 2009.

Gurtin M. *An introduction to continuum mechanics*. Academic Press, 1981.

Haley P. and Miksis M. The effect of the contact line on droplet spreading. *J. Fluid Mech.*, 223:57–81, 1991.

Hocking L. Sliding and spreading of thin two–dimensional drops. *Q. J. Mech. Appl. Math.*, 34:37–55, 1981.

Hughes T., Franca L., and Balestra M. A new finite element formulation for computational fluid dynamics: V. circumventing the Babuška–Brezzi condition. a stable Petrov-Galerkin formulation of the Stokes problem accommodating equal-order interpolations. *Comput. Methods Appl. Mech. Engrg.*, 59:85–99, 1986.

Idelsohn S., Mier-Torrecilla M., and Oñate E. Multi–fluid flows with the Particle Finite Element Method. *Comput. Methods Appl. Mech. Engrg.*, 198:2750–2767, 2009.

Kim D., Wong P., Park J., Levchenko A., and Sun Y. Microengineered platforms for cell mechanobiology. *Annual Review of Biomedical Engineering*, 11:203–233, 2009.

Lac E., Barthès-Biesel D., Pelekasis N., and Tsamopoulos J. Spherical capsules in three-dimensional unbounded Stokes flows: effect of the membrane constitutive law and onset of buckling. *Journal of Fluid Mechanics*, 516:303–334, 2004.

Marella S. and Udaykumar H. Computational analysis of the deformability of leukocytes modeled with viscous and elastic structural components. *Physics of Fluids*, 16(2):244–264, 2004.

Mc Kee S., Tomé M., Ferreira V., Cuminato J., Castelo A., Sousa F., and Mangiavacchi N. The MAC method. *Computers and Fluids*, 37:907–930, 2008.

Mut F., Buscaglia G., and Dari E. New mass-conserving algorithm for level set redistancing on unstructured meshes. *Journal of Applied Mechanics*, 73:1011–1016, 2006.

Pozrikidis C., editor. *Modeling and Simulation of Capsules and Biological Cells*. Mathematical Biology and Medicine Series. Chapman & Hall/CRC, 2003.

Ren W. and Weinan E. Boundary conditions for the moving contact line problem. *Physics of Fluids*, 19:022101, 2007.

Renardy M., Renardy Y., and Li J. Numerical simulation of moving contact line problems using a Volume–of–Fluid method. *J. Comput. Phys.*, 171:243–263, 2001.

Rothstein J. Slip on Superhydrophobic Surfaces. *Annu. Rev. Fluid Mech*, 42:89–109, 2010.

Scardovelli R. and Zaleski S. Direct numerical simulation of free-surface and interfacial flow. *Annu. Rev. Fluid Mech.*, 31:567–603, 1999.

Secomb T. and Skalak R. Surface flow of viscoelastic membranes in viscous fluids. *Quart. J. Mech. Appl. Math.*, 35:233–248, 1982.

Sethian J.A. and Smereka P. Level Set Methods for Fluids Interfaces. *Annual Rev. Fluid Mech.*, 35:341–372, 2003.

Skalak R., Tozeren A., Zarda R., and Chien S. Strain energy function of red blood cell membranes. *Biophysical Journal*, 13(3):245–264, 1973.

Spelt P. A level–set approach for simulations of flows with multiple moving contact lines with hysteresis. *Journal of Computational Physics*, 207:389–404, 2005.

Squires T. and Mason T. Fluid Mechanics of Microrheology. *Annual Review of Fluid Mechanics*, 42:413–438, 2010.

Squires T. and Quake S. Microfluidics: Fluid physics at the nanoliter scale. *Rev. Modern Phys.*, 77:977–1026, 2005.

Stone H., Stroock A., and Ajdari A. Engineering flows in small devices: Microfluidics toward a Lab-on-a-Chip. *Annu. Rev. Fluid Mech.*, 36:381–411, 2004.

Tezduyar T. Finite elements in fluids: Special methods and enhanced solution techniques. *Computers & Fluids*, 36:207–223, 2007.

Weinstein O. and Pismen L. Scale dependence of contact line computations. *Math. Model. Natural Phenom.*, 3:98–107, 2008.

Whitesides G. The origins and the future of microfluidics. *Nature*, 442:368–373, 2006.

Young N., Goldstein J., and Block M.J. The motion of bubbles in a vertical temperature gradient. *Journal of Fluid Mechanics*, 6:350–356, 1959.